

1 Role of Electronic Structure in the Morphotropic Phase Boundary  
2 of  $Tb_xDy_{1-x}Co_2$  Studied by First-principles Calculation

3 Dongyan Zhang<sup>1,2,a)</sup>, Sen Yang<sup>1,b)</sup>, Pangpang Wang<sup>3</sup>, Yu Wang<sup>1</sup>, Jieqiong Wang<sup>1</sup>,  
4 Xiaoping Song<sup>1</sup>

5  
6 <sup>1</sup>State Key laboratory for Mechanical Behavior of Materials and MOE Key Laboratory  
7 for Nonequilibrium synthesis and Modulation of Condensed Matter, Xi'an Jiaotong  
8 University, Xi'an 710049, People's Republic of China

9 <sup>2</sup>Graduate School of Advanced Technology and Science, the University of Tokushima,  
10 Tokushima 770-8506, Japan

11 <sup>3</sup>Institute for Materials Chemistry and Engineering, Kyushu University, Fukuoka  
12 812-8581, Japan

13

14 **Abstract**

15 Physically parallel to ferroelectric morphotropic phase boundary, a phase boundary  
16 separating two ferromagnetic phase of different crystallographic symmetries was found  
17 in  $Tb_xDy_{1-x}Co_2$ . High-resolution synchrotron XRD has been carried out to offer  
18 experimental evidence for  $Tb_xDy_{1-x}Co_2$ . It has been proved that  $Tb_xDy_{1-x}Co_2$  ( $0.6 < x < 0.7$ )

---

Author to whom correspondence should be addressed.

a) E-mail: [zhang@tokushima-u.ac.jp](mailto:zhang@tokushima-u.ac.jp)

b) E-mail: [yangsen@mail.xjtu.edu.cn](mailto:yangsen@mail.xjtu.edu.cn)

19 is a morphotropic phase boundary and that the crystal structures of tetragonal ( $x < 0.6$ )  
20 and rhombohedral ( $x > 0.7$ ) phase is distorted from a Laves Phase. Here, a first principles  
21 calculation provides a theoretical explanation on the origin of MBP in  $\text{Tb}_x\text{Dy}_{1-x}\text{Co}_2$  and  
22 is also provided for the question of why MPB occurs in  $\text{Tb}_x\text{Dy}_{1-x}\text{Co}_2$  alloys.

23

24

25  $RM_2$  (R: rare-earth element, M: transition metal) with the cubic Laves phase  
26 structure have attracted great attention for their variety of magnetic behavior<sup>1-3</sup>. All of  
27 them possess very similar lattice parameters<sup>4</sup> and exhibit a magnetic instability of the  
28 3d-subsystem due to the occupation of  $d$  and  $f$  orbitals<sup>5</sup>. Investigation on electronic  
29 structure of  $RM_2$  would improve our understanding on mechanism of their magnetic  
30 behavior. With the more results provided by experimental progress, the theoretical  
31 analysis made it possible to understand systematically the influence of the electronic  
32 structure on the magnetic properties<sup>6</sup>. A lot of researches<sup>7-10</sup> have been contributed on  
33 the theoretical and experimental investigation of  $RFe_2$ ,  $RCo_2$  and  $RNi_2$ . Especially for  
34  $Tb_xDy_{1-x}Co_2$ , a debate on the phase transition, if is the spin-reorientation transition also  
35 a border separating different crystal symmetries, has been continued for recent decades.  
36 The progress in this issue provides a deep insight into the nature of a fundamental  
37 concept in magnetism and provides a chance to study the transitions associated with  
38 electronic structure. Specially, the magnetic properties of cobalt are strongly depended  
39 on the rare-earth element .It offers an opportunity to investigate the occupation of  $d$  and  
40  $f$  orbitals and hybridization between them. As early as 1970s', Bloch<sup>11</sup> have pointed out  
41 that the cobalt moment is not intrinsic but induced in the d band by the exchange field  
42 due to the rare-earth, the behavior of transition in  $RCo_2$  have related the density of states

43 at the Fermi Level. Recently, Yang<sup>12-14</sup> has proved that a similar MPB situation exist in  
44 the ferromagnetic system as same as in the ferroelectric system, which have rectified the  
45 long standing mistake that the magnetic transition in  $Tb_xDy_{1-x}Co_2$  alloy is merely a  
46 reorientation of magnetization direction and there is no change in crystal symmetry.  
47 This promises to change our perception of how we think about the magnetic theory.  
48 Yang employed the high-resolution synchrotron XRD at the BL15XU NIMS beat line of  
49 Spring-8 to experimentally confirm the transition in  $Tb_xDy_{1-x}Co_2$  alloy. However, most  
50 of the theoretical explanations concerning the underlying mechanism of MPB have been  
51 phonological studies<sup>15, 16</sup>. In this letter, we investigated the electronic structure at the  
52 Fermi Level in  $Tb_xDy_{1-x}Co_2$  and clarified the origin of different ferromagnetic states  
53 corresponding to different crystal symmetries in  $Tb_xDy_{1-x}Co_2$  alloy by using first  
54 principles calculation. This work provides a theoretical explanation on the origin of  
55 MBP in  $Tb_xDy_{1-x}Co_2$  and is also provided for the question of why MPB occurs in  
56  $Tb_xDy_{1-x}Co_2$  alloys.

57 The calculations have been performed on the basis of spin-polarized DFT<sup>17, 18</sup> with  
58 the *ab initio* total energy program CASTEP<sup>19</sup>. For the exchange-correlation functional,  
59 we chose a local density approximation in the scheme of Ceperley and Alder<sup>20</sup>  
60 parameterized by Perdew and Zunger<sup>21</sup> denoted hereby CA-PZ. The spin interpolation

61 was used in this calculation. The self-consistent ground state of the system was  
62 determined using a band-by-band conjugate gradient technique to minimize the total  
63 energy of the system with respect to plane-wave coefficients. The electronic wave  
64 functions were obtained by the All Bands/EDFT scheme. A number of twelve valence  
65 electrons for each Dy atom ( $4f^{10}6s^2$ ) and eleven valence electrons for each Tb atom  
66 ( $4f^96s^2$ ) were taken into account. For each Co atom ( $3d^74s^2$ ), a number of nine valence  
67 electrons were employed and the formal spin state with 4 minority spin electrons was  
68 used as initial. The remaining core electrons together with the nuclei were described by  
69 pseudo-potentials in the framework of the PAW method<sup>22, 23</sup>. The one-electron  
70 Kohn-Sham wavefunctions as well as the charge density were expanded in a plane-wave  
71 basis set. The initial crystal structure model of cubic  $TB_xDy_{1-x}Co_2$  was build according  
72 to the previous research of the synchrotron XRD data<sup>14</sup>. Then, the Dy atoms in the  
73 supercell were gradually replaced and the cell was geometry optimized. In order to  
74 optimize the total energy of  $TB_xDy_{1-x}Co_2$  with Tetragonal symmetry, the crystal constant  
75  $c$  was only relaxed, and the other degrees of freedom were frozen. Similarly, in order to  
76 optimize the total energy of  $Tb_xDy_{1-x}Co_2$  with Rhombohedral symmetry, the crystal  
77 constant  $\alpha, \beta$  and  $\gamma$  were only relaxed, and the crystal constant  $a, b$  and  $c$  were fixed.

78 The lattice parameters for  $DyCo_2$  and  $TbCo_2$  at 0 K were extrapolated from the low

79 temperature X-ray analysis. A model of DyCo<sub>2</sub> in Laves phase was built with the lattice  
80 constant 7.12 Å<sup>24,25</sup>, and TbCo<sub>2</sub> in Laves phase with lattice constant 7.25 Å<sup>26</sup>. Then, the  
81 special symmetry employed on the model in Laves phase was canceled, and atoms in  
82 fractional coordinate were constrained. The crystal structure model of Tb<sub>x</sub>Dy<sub>1-x</sub>Co<sub>2</sub> with  
83 tetragonal symmetry or rhombohedral symmetry was modified from the Laves phase.  
84 Figure 1 shows the Laves phase configuration and the DOS for DyCo<sub>2</sub> with Laves phase.  
85 The crystallographic cell consists of an eight Tb<sub>x</sub>Dy<sub>1-x</sub>Co<sub>2</sub> formula unit. The total  
86 energies of Tb<sub>x</sub>Dy<sub>1-x</sub>Co<sub>2</sub> with Tetragonal symmetry were calculated with the  
87 compressing or stretching the *c* axis of Laves phase, and the total energies of  
88 Tb<sub>x</sub>Dy<sub>1-x</sub>Co<sub>2</sub> with Rhombohedral symmetry were calculated with altering the crystal  
89 constant  $\alpha, \beta$  and  $\gamma$  of Laves phase, synchronously. The *c*-axis was distorted to calculate  
90 the total energy of Tb<sub>x</sub>Dy<sub>1-x</sub>Co<sub>2</sub> with AMD symmetry. Otherwise, the angle was  
91 distorted to calculate the total energy of Tb<sub>x</sub>Dy<sub>1-x</sub>Co<sub>2</sub> with R-3M symmetry. The total  
92 energies of Tb<sub>x</sub>Dy<sub>1-x</sub>Co<sub>2</sub> with Tetragonal symmetry and Rhombohedral symmetry were  
93 shown in Figure 2. The horizontal coordinate indicates the distortion of *c*-axis. The  
94 positive value reveals the compression, and the negative value reveals the stretch. The  
95 ground state of the Tb<sub>x</sub>Dy<sub>1-x</sub>Co<sub>2</sub> was determined by considering spin configurations. All  
96 magnetic moments are aligned parallel in the ferromagnetic (FM) state for a

97 crystallographic cell, which is consistent with the FM nature of  $Tb_xDy_{1-x}Co_2$  under the  
98 Curie temperature.

99 Firstly, on the basis of atom configuration of Laves Phase, we investigated the  
100 electronic structure of  $DyCo_2$ . Figure 1 shows the Laves phase configuration and the  
101 DOS for  $DyCo_2$ . For one stoichiometric cell, twelve Co atoms locate at the vertex of a  
102 truncated tetrahedron, and one Dy atom locates at the center. The inset diagram is the  
103 schematic of spin electron configuration for Co atom in the truncated tetrahedron. In the  
104 view of classical crystal field theory, due to the Co's occupation at the vertex of a  
105 truncated tetrahedron rather than the central, the distortion of the crystal structure would  
106 not affect the spin electronic configuration of Co. It implies that there would be no  
107 structure phase transition in the case of Dy's substitute by Tb. It is significantly far from  
108 the experimental observation and our results of total energy calculation. Prof. Kimura<sup>27</sup>  
109 has developed an *Ab initio* calculation method to investigate the slight change of  
110 electronic structure in phase transition, which have been also proved by the  
111 experimental observation in the Martensitic phase transition of  $Ni_2Mn_{1+x}Sn_{1-x}$ . Even if  
112 the degenerate states of *d* orbits were not changed, the phase transition would also be  
113 predicted by the evolution of binding energy in the case of varying composites. We  
114 calculated the total energy variation of  $Tb_xDy_{1-x}Co_2$  caused by a tetragonal and

115 rhombohedra distortion from the Laves phase. The results for DyCo<sub>2</sub> (x=0) were shown  
116 in Figure 2a. The tetragonal phase is energetically favorable for DyCo<sub>2</sub>, as reported  
117 previously<sup>14</sup>. As shown in Figure 2a, the Laves phase, which is the parent phase for  
118 Tb<sub>x</sub>Dy<sub>1-x</sub>Co<sub>2</sub> above T<sub>c</sub>, tends to be unstable against tetragonal and rhombohedral  
119 distortion at low temperature. Significantly, DyCo<sub>2</sub> with tetragonal phase (AMD  
120 symmetry) manifested a favorite structure, when the c-axis was compressed 9.3%.  
121 Comparing to the energy evolution of DyCo<sub>2</sub> with rhombohedral phase, the tetragonal  
122 phase is optimal for DyCo<sub>2</sub>. Interestingly, the tetragonal phase tends to be unstable  
123 against rhombohedral distortion with increasing Tb composition<sup>26</sup>. For TbCo<sub>2</sub> (x=1), the  
124 minima in the total energy are located at the 86.5° along the rhombohedra distortion  
125 (R-3M). Figure 2b shows the total-energy variation of TbCo<sub>2</sub> (x=1) caused by the  
126 tetragonal or rhombohedra distortion from the Laves phase. The rhombohedra distortion  
127 is more energetically favorable than the tetragonal distortion. The theoretical results are  
128 consistent with the experimental observation<sup>26, 28</sup>, where the Tb<sub>x</sub>Dy<sub>1-x</sub>Co<sub>2</sub> alloy shows  
129 the different symmetry at the Dy-rich side and at the Tb-rich side. Table 1 shows the  
130 minima in the total energy of DyCo<sub>2</sub> and TbCo<sub>2</sub> with the tetragonal and rhombohedra  
131 symmetry. Such a phenomenon has perplexed the researchers for a long time, because  
132 Co atoms were ligands, occupying the vertex of a truncated tetrahedron and the spin

133 electronic configuration of  $f$  orbit for Tb or Dy is too complex to be investigated. To  
134 clarify this transition and gain further insight into the origin of the MPB observed in  
135  $\text{Tb}_x\text{Dy}_{1-x}\text{Co}_2$ , we have investigated the energy position of peak near  $E_F$ , which is  
136 apparently responsible for the MPB.

137 Figure 3 shows the total density of states near  $E_F$ , in the tetragonal phase of  
138  $\text{Tb}_x\text{Dy}_{1-x}\text{Co}_2$  for  $x=0, 0.1, 0.2, 0.3, 0.4, 0.5, 0.6$ , and in the rhombohedral phase of  
139  $\text{Tb}_x\text{Dy}_{1-x}\text{Co}_2$  for  $x=0.7, 0.8, 0.9, 1$ , respectively. A peak was found at about 0.6 eV  
140 below  $E_F$  in the DOS of  $\text{DyCo}_2$ . The peak in the DOS is predominantly composed of Co  
141 3d sub-orbitals, as pointed out in Figure 1. With an increase in the Tb composition, the  
142 peak structure shifts towards  $E_F$ . The peak shift can be attributed to the hybridization  
143 between the Co 3d orbitals and 4f orbitals of excess Tb atoms at Dy sites. It should be  
144 noted that the magnetic moment of  $\text{Tb}_x\text{Dy}_{1-x}\text{Co}_2$  was offered by Co. The substitute of  
145 Dy by Tb only changed the electrostatic potentials, which would affect the energy of Co  
146 3d sub-orbitals, rather than the degenerate states. Comparing to the Dy, Tb lacks a 4f  
147 electron. Considering the hybridization between the Co 3d orbitals and 4f orbitals of Tb  
148 or Dy, the peak in the DOS would shift towards  $E_F$ . Due to the limitation of the  
149 degenerate states of Co 3d orbitals, the peak would not shift through the  $E_F$ . However,  
150 due to the substitute of Dy by Tb, the peak shifts more and more close to the  $E_F$ . As a

151 result, the phase boundary was located between the Dy-rich side and the Tb-rich side.  
152 Our calculation predicted that such a phase boundary should locate around  $x=0.7$  for  
153  $\text{Tb}_x\text{Dy}_{1-x}\text{Co}_2$ , which well agrees the previous experimental observation<sup>14</sup>. Crossing the  
154 phase boundary, the peak would shift away from the  $E_F$ , as the composite of Tb  
155 increases. Such a calculation results could be simply understood via studying the  
156 relationship between number of valence electrons (NVE) and  $E_F$ . If the Dy site is  
157 substituted by a Tb atom, a smaller NVE would be expected to result a drop of  $E_F$ . The  
158 abnormal shift of the peak in the vicinity of  $E_F$  is attributed to the variation of NVE.  
159 However, the peak corresponding to Co  $3d$  orbit is prohibited to cross  $E_F$ . Therefore, the  
160 phase transition occurs, when the abnormal shift is reversed.

161 The most interesting feature of the MPB composition is the magneto-responsive  
162 properties. Certainly, the MPB would separate two composite dependence free energy  
163 evolutions in accordance with symmetry. Figure 4 shows the composition dependence  
164 of integrated spin density and Fermi energy. Accompanying the free energy varying, the  
165 integrated |spin density| shows a step at the MPB composition, as shown in Figure 4a.  
166 The integrated |spin density| denotes the spontaneous magnetization, which is also  
167 superiority at Tb-rich side in the experimental observation<sup>14</sup> as shown in the inset of  
168 Figure 4a. Figure 4b shows the variation of Fermi level as a function of the composite.

169 It is significant that a transition occurred at the MPB composition. The MPB separated  
170  $Tb_xDy_{1-x}Co_2$  into different symmetries.

171 In conclusion, we proved a magnetic MPB in a ferromagnetic  $Tb_xDy_{1-x}Co_2$  system,  
172 which separates two magnetic phase with different crystal symmetries. The MPB leads  
173 to a significant variation in magnetic properties and in crystal structure. The calculation  
174 reveals that the MPB is a boundary of T and R phase and is a thermodynamically  
175 bistable states. The proving of MPB in ferromagnetic system may provide an effective  
176 approach for developing highly magnetostrictive materials, and suggests the possibility  
177 of MPB in other ferroic systems. The calculation of MPB provides an effective  
178 approach to search the MPB composition. It also provides a new insight into the nature  
179 of magnetism and phase transition.

180

## 181 **Acknowledgement**

182 This research was supported by the National Basic Research Program of China  
183 (Grant No. 2012CB619401), National Science Foundation of China (Grant Nos.  
184 51222104 and 51071117) and Fundamental Research Funds for Central Universities.

185

186

187 **References**

188

- 189 1. M. Cyrot and M. Lavagna, *J. Phys. France* **40** (8), 763-771 (1979).
- 190 2. P. d. I. Presa, S. Müller, A. F. Pasquevich and M. Forker, *Journal of Physics:*  
191 *Condensed Matter* **12** (14), 3423 (2000).
- 192 3. E. Burzo, L. Chioncel, R. Tetean and O. Isnard, *Journal of Physics: Condensed*  
193 *Matter* **23** (2), 026001 (2011).
- 194 4. R. L. Cohen, K. W. West, F. Oliver and K. H. J. Buschow, *Phys Rev B* **21** (3),  
195 941-944 (1980).
- 196 5. H. Yamada, *Physica B+C* **149** (1–3), 390-402 (1988).
- 197 6. Y. Kucherenko, S. L. Molodtsov, A. N. Yaresko and C. Laubschat, *Phys Rev B*  
198 **70** (4), 045105 (2004).
- 199 7. K. H. J. Buschow and R. P. van Staple, *Journal of Applied Physics* **41** (10),  
200 4066-4069 (1970).
- 201 8. J. S. Kang, K. Kang and B. I. Min, *Physica B: Condensed Matter* **230–232** (0),  
202 497-499 (1997).
- 203 9. M. Onak, P. Guzdek, P. Stoch, J. Chmista, M. Bednarski, A. Pańta and J. Pszczoła,  
204 *Journal of Alloys and Compounds* **433** (1–2), 53-58 (2007).
- 205 10. C. M. Chaves, A. L. de Oliveira, N. A. de Oliveira and A. Troper, *Journal of*

- 206 Magnetism and Magnetic Materials **323** (6), 881-884 (2011).
- 207 11. D. Bloch, D. M. Edwards, M. Shimizu and J. Voiron, Journal of Physics F:  
208 Metal Physics **5** (6), 1217 (1975).
- 209 12. S. Yang, X. B. Ren and X. P. Song, Phys Rev B **78** (17) (2008).
- 210 13. S. Yang and X. B. Ren, Phys Rev B **77** (1) (2008).
- 211 14. S. Yang, H. X. Bao, C. Zhou, Y. Wang, X. B. Ren, Y. Matsushita, Y. Katsuya, M.  
212 Tanaka, K. Kobayashi, X. P. Song and J. R. Gao, Phys Rev Lett **104** (19) (2010).
- 213 15. P. Entel, V. D. Buchelnikov, V. V. Khovailo, A. T. Zayak, W. A. Adeagbo, M. E.  
214 Gruner, H. C. Herper and E. F. Wassermann, Journal of Physics D: Applied  
215 Physics **39** (5), 865 (2006).
- 216 16. S. Wei, X. Song, S. Yang, J. Deng and Y. Wang, Shenzhen, China, 2011  
217 (unpublished).
- 218 17. P. Hohenberg and W. Kohn, Physical Review **136** (3B), B864-B871 (1964).
- 219 18. H. Eschrig, G. Seifert and P. Ziesche, Solid State Communications **56** (9),  
220 777-780 (1985).
- 221 19. S. J. Clark, M. D. Segall, C. J. Pickard, P. J. Hasnip, M. I. J. Probert, K. Refson  
222 and M. C. Payne, Zeitschrift für Kristallographie **220** (5-6-2005), 567-570  
223 (2005).

224 20. D. M. Ceperley and B. J. Alder, Phys Rev Lett **45** (7), 566-569 (1980).

225 21. J. P. Perdew and A. Zunger, Phys. Rev. B **23** (10), 5048--5079 (1981).

226 22. P. E. Blöchl, Phys Rev B **50** (24), 17953-17979 (1994).

227 23. G. Kresse and D. Joubert, Phys Rev B **59** (3), 1758-1775 (1999).

228 24. P. Stoch, J. Pszczoła, P. Guzdek, J. Chmist and A. Pańta, Journal of Alloys and  
229 Compounds **394** (1–2), 116-121 (2005).

230 25. K. Gu, J. Li, W. Ao, Y. Jian and J. Tang, Journal of Alloys and Compounds **441**  
231 (1–2), 39-42 (2007).

232 26. V. Goldberg-Murmis, U. Atzmony and M. P. Dariel, J Mater Sci **15** (1), 127-130  
233 (1980).

234 27. M. Ye, A. Kimura, Y. Miura, M. Shirai, Y. T. Cui, K. Shimada, H. Namatame, M.  
235 Taniguchi, S. Ueda, K. Kobayashi, R. Kainuma, T. Shishido, K. Fukushima and  
236 T. Kanomata, Phys Rev Lett **104** (17), 176401 (2010).

237 28. S. Yang and X. Ren, Phys Rev B **77** (1), 014407 (2008).

238

239

240

241

242 **Table list**

243 Table 1. Comparison of total energy between DyCo<sub>2</sub> and TbCo<sub>2</sub> with the tetragonal and  
244 rhombohedra symmetry

245 Table 1. Comparison of total energy between DyCo<sub>2</sub> and TbCo<sub>2</sub> with the tetragonal and rhombohedra  
246 symmetry

	Total energy (eV)		Favorable structure
	Tetragonal	Rhombohedral	
DyCo <sub>2</sub>	-48607.9	-48607.2	Tetragonal (a=7.12 Å, c=6.46Å)
TbCo <sub>2</sub>	-44720.9	-44721.1	Rhombohedral (a=7.25 Å, α=86.5°)

247

248

249 **Captions**

250 Figure 1. The truncated tetrahedron configuration and the DOS for DyCo<sub>2</sub> with Laves  
251 phase.

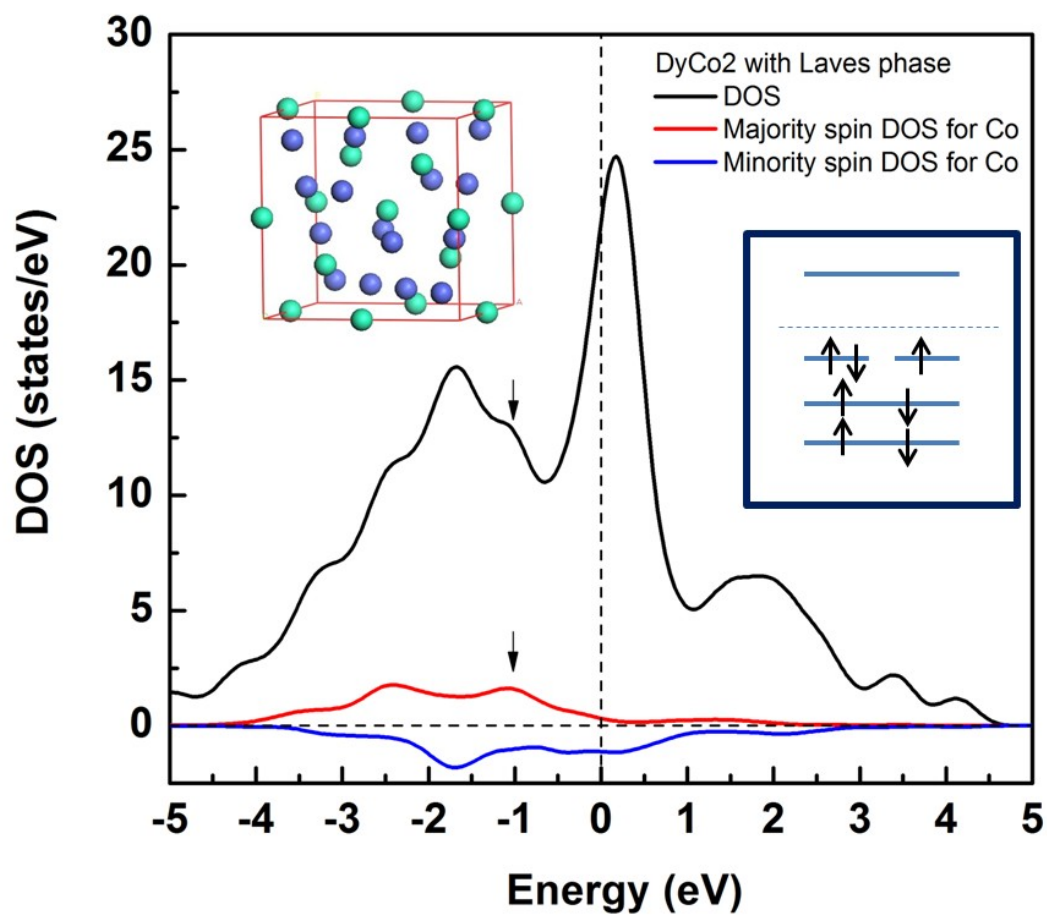
252 Figure 2. (a). The total energies of DyCo<sub>2</sub> with Tetragonal symmetry and Rhombohedral  
253 symmetry. (b). The total energies of TbCo<sub>2</sub> with Tetragonal symmetry and  
254 Rhombohedral symmetry

255 Figure 3. The total density of states near  $E_F$ , in the tetragonal phase of Tb<sub>x</sub>Dy<sub>1-x</sub>Co<sub>2</sub> for  
256  $x=0, 0.1, 0.2, 0.3, 0.4, 0.5, 0.6$ , and in the rhombohedral phase of Tb<sub>x</sub>Dy<sub>1-x</sub>Co<sub>2</sub>  
257 for  $x=0.7, 0.8, 0.9, 1$ , respectively.

258 Figure 4. Composition dependence of physical properties in relation with MPB.

259

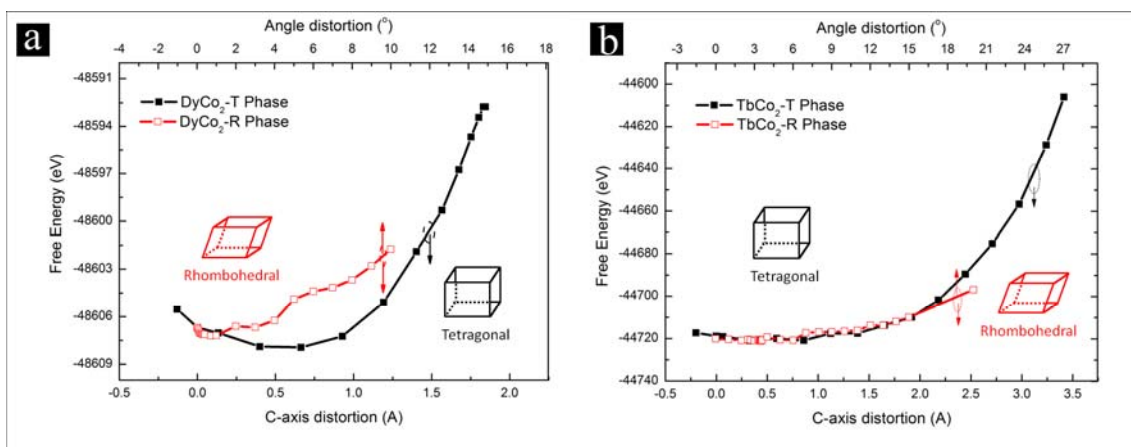
260



261

262

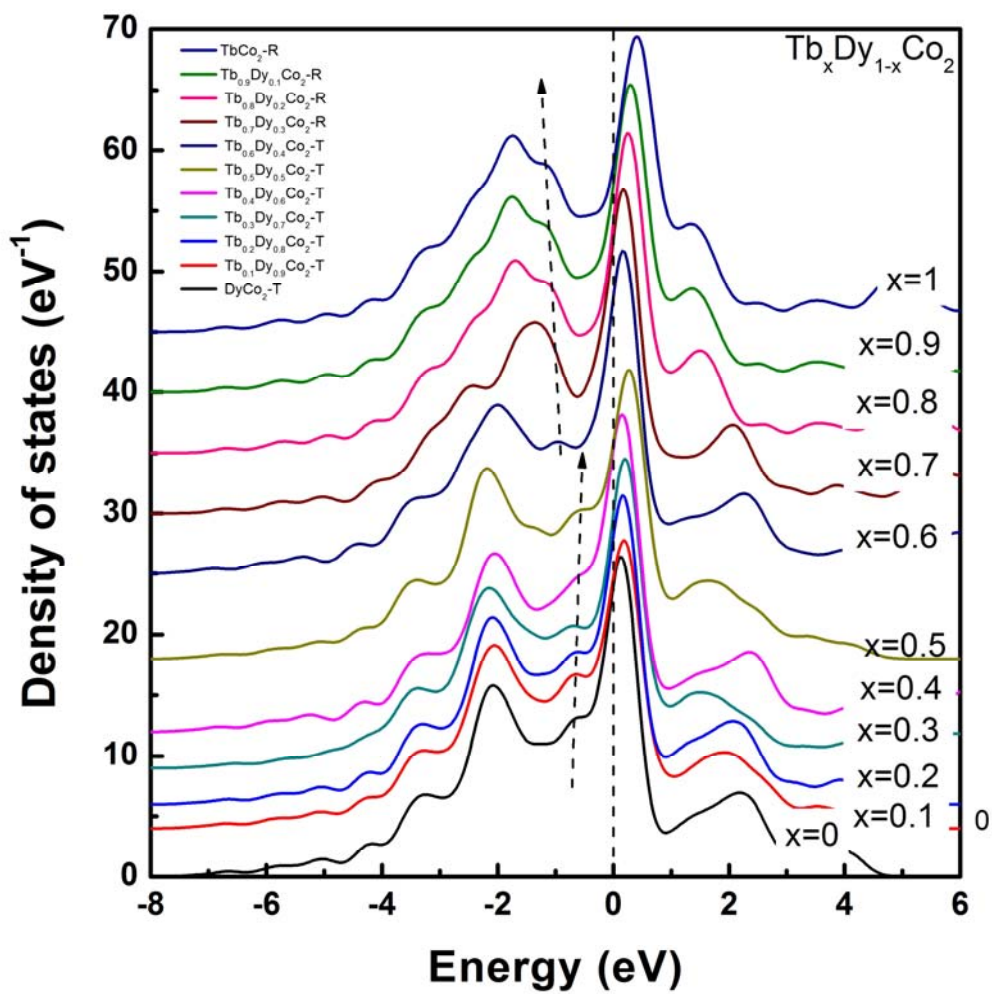
Figure 1



263

264

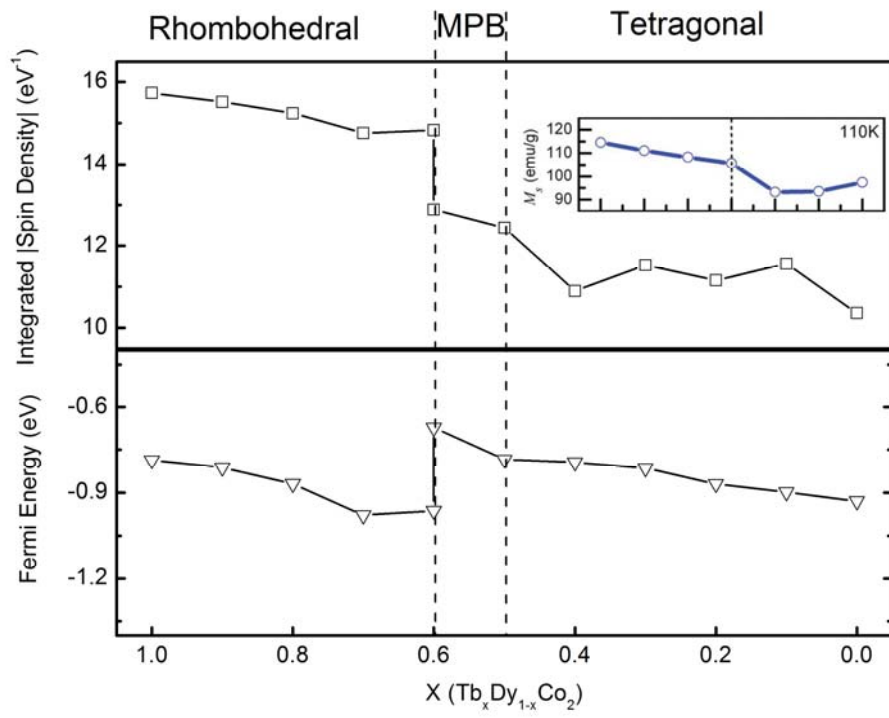
Figure 2



265

266

Figure 3



267

268

Figure 4